Int. J. Heat Mass Transfer. Vol. 30, No. 3, pp. 437–447, 1987
Printed in Great Britain

0017–9310/87 $3.00 + 0.00
Pergamon Journals Ltd.

Application of statistical narrow-band model to coupled radiation and convection at high temperature

A. SOUFIANI and J. TAINE

Laboratoire d'Energétique Moléculaire et Macroscopique, Combustion, Laboratoire du C.N.R.S. et de l'E.C.P., Ecole Centrale des Arts et Manufactures, 92295 Châtenay-Malabry Cedex, France

(*Received* 30 *October* 1985 *and in final form* 7 *May* 1986)

Abstract—The use of wide-band or gray-gas models in coupled heat transfer calculations frequently leads to significant errors due to spectral correlations between the emitted flux intensity and gas transmissivity. In the present study, the random statistical narrow-band model with the exponential-tailed-inverse distribution and the Curtis–Godson approximation are used with a $25\,cm^{-1}$ spectral resolution; our parameters are generated from a line-by-line calculation. Coupled dynamic and energy equations are solved for an emitting and absorbing laminar gas flow between two parallel walls at fixed temperature. The influence of radiative and thermophysical property variations with temperature is analysed for H_2O–air mixtures under strong temperature gradients. A large range of optical thickness is studied. Different temperature and heat flux profiles are found when the walls are heated or cooled. Finally, results obtained with the statistical narrow-band model and the exponential wide-band model are compared.

1. INTRODUCTION

MANY applications of interest (rocket and aircraft propulsion, boilers and furnaces, nuclear reactors, etc.) involve infra-red active gas mixtures at high temperature. In these situations, the gas–gas and gas–wall radiative transfers are important or predominant. Coupled radiative–conductive and convective heat transfer in flowing systems has thus received considerable attention in the last 20 years.

Some authors use the gray-gas approximation [1–4] or the Planck or Rosseland mean absorption coefficient [5–7] to model the radiative properties of gases. More accurate approaches [8–17] take into account the discrete absorption bands with the exponential wide-band model due to Edwards and Menard [18] and use sometimes the Tien–Lowder correlation [19, 20]. Nichols [21] used a random-statistical wide-band model with uniform intensity distribution and assumed a constant blackbody intensity over each absorption band. Recent developments in gas molecular spectroscopy have improved knowledge of radiative properties. A line-by-line calculation has been developed for H_2O–CO_2–CO transparent gas mixtures and for temperatures up to 2000 K [22, 23], but its use is impractical for most engineering applications. The accuracy of low resolution radiative models has been studied in detail in a previous publication [24] for a combined conductive and radiative transfer in a planar gas medium. Results obtained for H_2O–air and CO_2–air mixtures show that wide-band models can lead to significant temperature and flux discrepancies, because spectral correlations between gas transmissivity and emitted flux intensities exist even inside an absorption band.

On the other hand, the frequent use of constant thermophysical fluid properties [1–3, 9, 10], and of dynamical or thermal established profiles [1–5, 9, 10, 13], or linearized radiative fluxes [16, 17] can only be justified in the case of small temperature differences.

We propose, in this paper, a laminar channel flow model, for the coupled conductive, radiative and convective transfer, which does not require the previous approximations. The strong temperature difference imposed between the walls and the fluid requires the use of temperature-dependent fluid physical properties, and of an accurate radiative modelling of non-isothermal medium (high-resolution correlations between absorption and emission spectra). The radiative treatment is based on a random-statistical narrow-band model with a $25\,cm^{-1}$ resolution and on the Curtis–Godson approximation. The flow equations and the energy conservation equation are solved simultaneously in order to describe the interaction between temperature, radiative and conductive fluxes and velocity profiles. Dynamical and thermal entrance regions are studied either in the case of weak interaction (predominance of conductive or radiative mode) and when the two modes are of the same order of magnitude. Results obtained when cooling and when heating the absorbing and emitting fluid are then compared. Finally, the results obtained with the exponential wide-band model due to Edwards are compared to those obtained with the statistical narrow-band model in a wide range of optical thicknesses.

2. BASIC EQUATIONS

2.1. *Flow equations*

We consider a steady laminar flow between two parallel walls at fixed temperature T_w. The walls

NOMENCLATURE

A	matrix corresponding to geometrical integrated transmissivity
a, c	thermal conductivity between calculation grids
B	vector corresponding to radiative intensities
b	$(a + c)/2$
C_p	specific heat at constant pressure
d	length of column
E	distance between the walls
I^b	blackbody intensity
$\bar{k}$	mean line intensity to spacing ratio inside $\Delta\nu$
$\dot{m}$	mass flow rate per unit area
M	number of lines inside $\Delta\nu$
N	number of gas layers plus two
P	pressure
q_R	radiative flux
S_m	intensity of the mth absorption line
T	local temperature
T_b	mixed mean temperature
u	axial velocity
v	transverse velocity
x	flow direction
x_i	molar fraction of species i
X_d	path length, $x_i P d$
y	transverse direction.

Greek symbols

$\bar{\beta}$	mean line width to spacing ratio
γ	half-width of an absorption line
$\bar{\delta}$	equivalent line spacing
$\Delta\nu$	low resolution spectral range
ε	emissivity
λ	molecular thermal conductivity
μ	viscosity or angle cosine in radiative developments
ν	wave number
ρ	density
τ	transmissivity
φ	flux transfered to fluid.

Subscripts

y	transverse component
0	inlet conditions
ν	monochromatic quantity
j, l, m	discretization over the y-direction
cv	convective
cd	conductive
R	radiative.

Superscripts

$\bar{\ }$	mean properties over the spectral range $\Delta\nu$
i	discretization over the x-direction
k	spectral band.

are diffuse but not necessarily gray. The fluid is a homogeneous absorbing, emitting and non-scattering gas mixture in local thermodynamic equilibrium. Viscous dissipation effects and axial diffusion are neglected in the energy equation; the contributions of transverse convection are assumed to be very small compared to those of axial convection both in the momentum and in the energy conservation equations. We also neglect the axial dissipation of the radiative flux in comparison with its transverse dissipation; De Soto [9] discusses this assumption and shows that it is justified for a downstream location three times greater than the hydraulic diameter. Under these conditions, the basic equations of the flow reduce to:

continuity

$$\frac{\partial}{\partial x}(\rho u) + \frac{\partial}{\partial y}(\rho v) = 0; \tag{1}$$

momentum equation projected on the axial direction

$$\rho u \frac{\partial u}{\partial x} = -\frac{\partial P}{\partial x} + \frac{\partial}{\partial y}\left(\mu \frac{\partial u}{\partial y}\right); \tag{2}$$

energy conservation

$$\rho C_p u \frac{\partial T}{\partial x} = u \frac{\partial P}{\partial x} + \frac{\partial}{\partial y}\left(\lambda \frac{\partial T}{\partial y}\right) - \frac{\partial q_{Ry}}{\partial y}. \tag{3}$$

The boundary conditions are

$$T(x, 0) = T(x, E) = T_w \tag{4}$$

$$u(x, 0) = u(x, E) = 0 \tag{5}$$

where E is the distance between the walls. The inlet conditions can be of any kind: two conditions will be studied here

$$T(0, y) = T_0 \text{ and } u(0, y) = \frac{\dot{m}}{\rho(T_0)} = u_0 \tag{6}$$

$$T(0, y) = T_0 \text{ and } u(0, y) = \frac{6\dot{m}}{E^2 \rho(T_0)} y(E - y) \tag{7}$$

where $\dot{m}$ is the mass flow rate per unit cross-sectional area. The first conditions, equation (6), enable the study of radiation effects on the dynamic establishment of the flow while the second correspond to a fully developed, isothermal flow at the inlet.

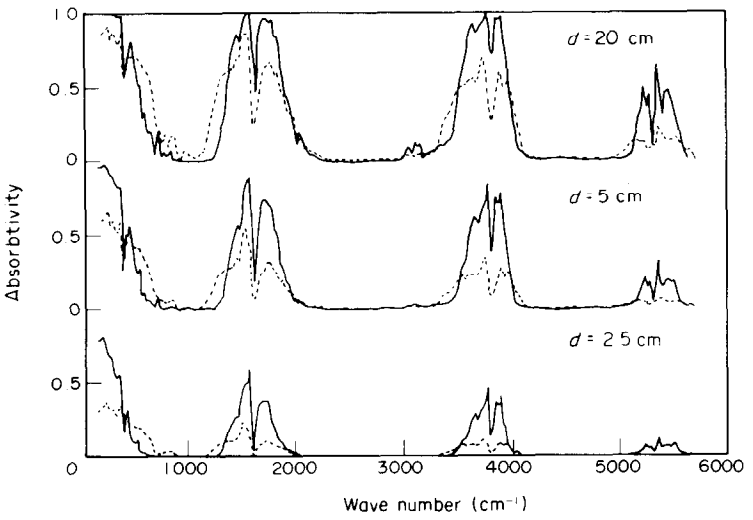

FIG. 1. Absorption spectra of pure H_2O at: ——, 400 K; and – – – –, 1200 K; for different column lengths d.

2.2. *Radiative model*

Various wide- and narrow-band radiative models have been recently tested with a line-by-line calculation for conducting and radiating CO_2–air and H_2O–air mixtures [24]. The most accurate temperature and flux distributions are obtained with the narrow-band model which assumes the absorption lines to be randomly placed and the intensities to obey an exponential-tailed-inverse distribution. The transmissivity of a homogeneous column, averaged over the spectral range $\Delta\nu$, is given by

$$\bar{\tau}_\nu = \exp\left[-\frac{\bar{\beta}}{\pi}\left(\sqrt{1+\frac{2\pi x_i P d\bar{k}}{\bar{\beta}}}-1\right)\right] \quad (8)$$

where x_i, P and d are the molar fraction of the absorbing species i, total pressure and length of the column, respectively. Parameters $\bar{k}$ and $\bar{\beta}$ are given by

$$\bar{\beta} = 2\pi\bar{\gamma}/\bar{\delta} \quad (9)$$

$$\bar{\gamma} = \frac{1}{M}\sum_{m=1}^{M}\gamma_m \quad (10)$$

$$\bar{\delta} = \bar{k}\bar{\gamma}\Big/\left(\Delta\nu^{-1}\sum_{m=1}^{M}\sqrt{(S_m\gamma_m)}\right)^2 \quad (11)$$

$$\bar{k} = \frac{1}{\Delta\nu}\sum_{m=1}^{M}S_m. \quad (12)$$

Here γ_m and S_m are the half-width and the integrated intensity of line m respectively; M is the number of lines inside $\Delta\nu$. The mean parameters of this model, generated from a line-by-line calculation, have been published for H_2O and CO_2 [23, 24]. As an illustration, Fig. 1 shows the absorption spectra of pure water vapour at 400 and 1200 K, for three column lengths, in the 150–6000 cm^{-1} range (infra-red range used in this study) and with a 25 cm^{-1} resolution. These spectra are related to three flows studied further: $d = 20$ cm corresponds to a predominantly radiative transfer; $d = 2.5$ cm refers to a predominantly conductive transfer, and $d = 5$ cm to similar order of magnitude of the two modes.

For a non-isothermal or non-homogeneous column, the Curtis–Godson approximation leads to very accurate results when pressure gradients are moderate [24]. This approximation assigns to such a column an equivalent homogeneous column with suitably defined spectroscopic parameters $\bar{k}'$ and $\bar{\beta}'$ [20]

$$X_d\bar{k}' = \int_0^{X_d}\bar{k}\,dX \quad (13)$$

$$X_d\bar{k}'\bar{\beta}' = \int_0^{X_d}\bar{k}\bar{\beta}\,dX \quad (14)$$

where X_d is the product x_iPd. Radiation from this equivalent column is then calculated from equation (8).

3. METHOD OF SOLUTION

3.1. *General method*

The frequently used numerical methods for the solution of partial differential equations including radiation effects are: (i) finite differences [12, 13, 25, 26], (ii) finite elements [4, 27] for more complex geometries and (iii) series expansion [11, 16].

We have retained a semi-implict finite-difference method for the solution of the parabolic equations (2) and (3). As pointed out by De Soto [9], dimensionless treatment of these equations has a very limited utility in the case of realistic gas band radiation and when thermophysical properties are temperature dependent; the resolution is thus undertaken in dimensional

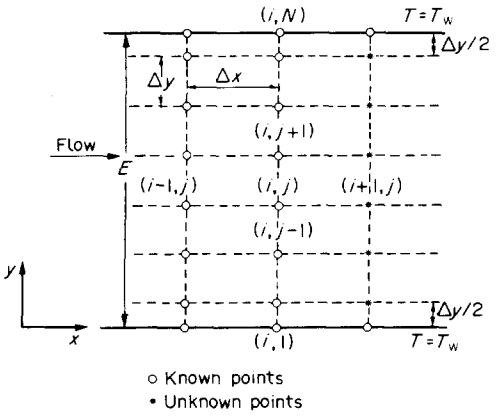

FIG. 2. Mesh network for finite differences.

form. The following sequences are used to obtain all the variables at each successive cross-sectional plane (Fig. 2):

(1) The transverse radiative dissipation $(\partial q_{Ry}/\partial y)^{i+1}$ at section $(i+1)$ is calculated by using the temperature field $(T)^i$ at section i.

(2) The energy equation is solved with the previous axial velocity field $(u)^i$ and the previous pressure drop $(\partial P/\partial x)^i$.

(3) The temperature profile $(T)^{i+1}$ is used to calculate new thermophysical and radiative fluid properties.

(4) The velocity field $(u)^{i+1}$ is calculated with the previous pressure drop $(\partial P/\partial x)^i$ and assuming that pressure is uniform over the cross-sectional plane [28].

(5) Pressure drop $(\partial P/\partial x)^{i+1}$ is adjusted in the momentum equation in order to satisfy the integrated continuity equation; an iteration over steps (4) and (5) is then made until the mass flow rate $\dot{m}$ is conserved

$$\int_0^E \rho u \, dy = E\dot{m}. \tag{15}$$

An interation over all these sequences could be used, but results show that the low variations of temperature, velocity and thermophysical properties on the axial step Δx, of a few millimetres, make the first calculation sufficient.

Discretization of energy and momentum equations leads to two linear systems which are solved by tridiagonal matrix inversion with Gaussian elimination.

Calculations without radiation (dry air) lead to a good agreement with the results obtained by Shade and McEligot [32]; discrepancies of about 5% on the Nusselt number, based on the bulk temperature, are due to the different thermophysical property models.

3.2. *Discretization*

Temperature-dependent thermophysical properties are linearized between three consecutive cross-sections. For instance, we set for thermal conductivity

$$a_j^i = \tfrac{1}{2}(\lambda_{j-1}^i + \lambda_j^i); \quad b_j^i = \tfrac{1}{4}(\lambda_{j-1}^i + 2\lambda_j^i + \lambda_{j+1}^i);$$
$$c_j^i = \tfrac{1}{2}(\lambda_j^i + \lambda_{j+1}^i); \tag{16}$$

and

$$a_j^{i+1} = 2a_j^i - a_j^{i-1}; \quad b_j^{i+1} = 2b_j^i - b_j^{i-1};$$
$$c_j^{i+1} = 2c_j^i - c_j^{i-1}. \tag{17}$$

Indices i and j correspond to axial and transverse directions respectively, as shown in Fig. 2. The finite-difference approximation of the energy equation for a wall non-adjacent node is then

$$\frac{a_j^{i+1}}{2\Delta y^2} T_{j-1}^{i+1} - \left(\frac{b_j^{i+1}}{\Delta y^2} + \frac{(\rho u)_j^i C_{pj}^i}{\Delta x}\right) T_j^{i+1}$$
$$+ \frac{C_j^{i+1}}{2\Delta y^2} T_{j+1}^{i+1} = -u_j^i \left(\frac{\partial P}{\partial x}\right)^i - \frac{a_j^i}{2\Delta y^2} T_{j-1}^i$$
$$+ \left(\frac{b_j^i}{\Delta y^2} - \frac{(\rho u)_j^i C_{pj}^i}{\Delta x}\right) T_j^i - \frac{c_j^i}{2\Delta y^2} T_{j+1}^i - \Delta q_{Rj}^i \tag{18}$$

where Δq_{Rj}^i is the transverse radiative dissipation term.

The absorption bands of the gas are divided into intervals of $\Delta\nu = 25\,\text{cm}^{-1}$ width, characterized by the superscript k, over which the blackbody spectral intensity I_ν^b is constant. Then Δq_{Rj}^i is given by

$2 \leqslant j \leqslant N-1$,

$$\Delta y \Delta q_{Rj}^i = \sum_k \left(A_{j1}^k B_1^k + A_{jN}^k B_N^k + \sum_{m=2}^{N-1} A_{jm}^k B_m^k \right). \tag{19}$$†

Values $m = 1$ and N designate the walls while j and m different from 1 and N are related to the gas layers around nodes j and m, respectively. For gaseous layer m, B_m^k is proportional to the emitted flux in range $\Delta\nu$

$$B_m^k = \pi \Delta\nu I_{\nu k}^b(T_m^i). \tag{20}$$

$[A_{jm}^k]$ is a symmetrical matrix; each of its terms accounts for geometrical integrated radiative properties between the two planes $(j-1/2)$ and $(m+1/2)$. For two non-adjacent gas layers $(m \geqslant j+2)$, A_{jm}^k is related to the flux emitted by layer m and directly absorbed by layer j, i.e.

$$A_{jm}^k = 2\int_0^1 \mu \int_{\nu^k - \Delta\nu/2}^{\nu^k + \Delta\nu/2} \varepsilon_{\nu_j} \cdot \tau_{\nu_{j+1}} \cdot \ldots \cdot \tau_{\nu_{m-1}} \cdot \varepsilon_{\nu_m} \, d\nu \, d\mu \tag{21}$$‡

where μ is the cosine of the angle between the $0y$ axis and the direction of an elementary column. ε_{ν_i} and τ_{ν_i} are respectively the spectral emissivity and trans-

†The meaning of the different terms in this equation are given in ref. [24], but it is repeated here in order to facilitate reading.

‡Superscript k is omitted in τ and ε notations.

missivity of a column of length $\Delta y/\mu$ of the layer. Spectral integration of equation (21) leads to

$$A^k_{jm} = 2\int_0^1 (\bar\tau_{v_{j+1,m-1}} - \bar\tau_{v_{j,m-1}} - \bar\tau_{v_{j+1,m}} + \bar\tau_{v_{j,m}})\mu\,d\mu \quad (22)$$

where $\bar\tau_{v_{j,m}}$ is the correlated transmissivity, averaged over Δv, of the non-isothermal column of length $(m-j+1)\,\Delta y/\mu$ between layers m and j. For two adjacent layers

$$A^k_{j,j+1} = 2\int_0^1 (1 - \bar\tau_{v_j} - \bar\tau_{v_{j+1}} + \bar\tau_{v_{j,j+1}})\mu\,d\mu. \quad (23)$$

The term A^k_{jj} accounts for emission of layer j and is given by

$$A^k_{jj} = -4\int_0^1 (1 - \bar\tau_{v_j})\mu\,d\mu. \quad (24)$$

Terms A^k_{j1} and A^k_{jN} of equation (19) correspond to the gas–wall radiation transfer, i.e.

$$A^k_{1,2} = -\tfrac{1}{2}A^k_{2,2} \quad (25)$$

$$3 \leqslant j \leqslant N-1, \qquad A^k_{1,j} = 2\int_0^1 (\bar\tau_{v_{2,j}} - \bar\tau_{v_{1,j}})\mu\,d\mu \quad (26)$$

$$A^k_{N-1,N} = -\tfrac{1}{2}A^k_{N-1,N-1} \quad (27)$$

$$2 \leqslant j \leqslant N-2,$$

$$A^k_{j,N} = 2\int_0^1 (\bar\tau_{v_{j+1,N-1}} - \bar\tau_{v_{j,N-1}})\mu\,d\mu. \quad (28)$$

The last term of the matrix accounts for the wall–wall exchange, i.e.

$$A^k_{1N} = 2\int_0^1 \bar\tau_{v_{2,N-1}}\mu\,d\mu. \quad (29)$$

The previous set of equations is completed by the relation which gives the radiosities B^k_1 and B^k_N of the diffuse walls

$$B^k_1 = B^k_N = \varepsilon_{vk}\pi\Delta v I^b_{vk}(T_w) + (1 - \varepsilon_{vk})\sum_{i=2}^{N} A^k_{1i}B^k_i \quad (30)$$

where ε_{vk} is the spectral emissivity of the wall.

The determination of the radiative dissipation involves the calculation of a layer–layer transmissivity matrix with terms as $\int_0^1 \bar\tau_{v_{jm}}\mu\,d\mu$. This geometrical integration leads, with a gray gas or a box model, to the integro-exponential function E_3; with the random statistical model used here, we find

$$\int_0^1 \bar\tau_{v_{jm}}\mu\,d\mu = \int_0^1 \exp\left[-\frac{\bar\beta'}{\pi}\left(\sqrt{\left(1 + \frac{2\pi x_i P\bar k'(|m-j|+1)\Delta y}{\mu\bar\beta'}\right)} - 1\right)\right]\mu\,d\mu \quad (31)$$

where $\bar k'$ and $\bar\beta'$ are the mean Curtis–Godson parameters averaged over the optical path of length $(|m-j|+1)\Delta y/\mu$. Numerical integration for each flow cross-section and each pair (j,m) requires substantial computer time. The following approximation has been used

$$\int_0^1 \exp\left[-X_1\left(\sqrt{\left(1 + \frac{X_2}{\mu X_1}\right)} - 1\right)\right]\mu\,d\mu = \tau + 0.0425\cos(\pi(\tau - 0.5)) \times \exp(-2(\tau - 0.5)^2)\exp(-X_1) \quad (32)$$

where

$$X_1 = \frac{\bar\beta'}{\pi}; \qquad X_2 = 2x_i P\bar k'(|m-j|+1)\Delta y;$$

$$\tau = E_3\left(X_1\left(\sqrt{\left(1 + \frac{X_2}{X_1}\right)} - 1\right)\right). \quad (33)$$

The integro-exponential function E_3 is given by

$$E_3(z) = \int_0^1 \exp(-z/\mu)\mu\,d\mu \quad (34)$$

and has been calculated using a series expansion[29].

The approximation in equation (32) leads to a maximum error of 1% for the variation ranges of $\bar k'$ and $\bar\beta'$ involved for H_2O. These mean parameters have been tabulated at ten intermediate temperatures and a simple interpolation is used for any other temperature.

Table 1. Thermophysical properties of air (1) and water vapour (2)

Z	Unit			m
λ_1	$W\,m^{-1}\,K^{-1}$	0	3.76×10^{-4}	0.747
λ_2		−0.0166	1.05×10^{-4}	1
μ_1	$10^{-6}\,N\,s\,m^{-2}$	1	0.4837	0.639
μ_2		−3.071	0.0407	1
C_{p_1}	$J\,kg^{-1}\,K^{-1}$	930	0.2073	1
C_{p_2}		1680	0.600	1

3.3. *Thermophysical properties*

Thermophysical properties of a mixture of air, noted 1, and H_2O, noted 2, obtained from a compilation of different values [30, 31], are given by equations (35)–(38) and Table 1, where x_i $(i = 1, 2)$ is the molar fraction of species i. Viscosity μ, thermal conductivity λ and specific heat at constant pressure C_p are approximated with 1% maximum error in the 400–1200 K temperature range by

$$\mu = \mu_1/[1 + (x_2/x_1)\phi_{12}] + \mu_2/[1 + (x_1/x_2) \times 1.608\phi_{12}(\mu_2/\mu_1)] \quad (35)$$

$$\phi_{12} = 0.219(1 + 0.888\sqrt{(\mu_1/\mu_2)})^2 \quad (36)$$

$$\lambda = \lambda_1/[1 + (x_2/x_1)(0.955 - 0.1417x_1)] + \lambda_2/[1 + (x_1/x_2)(0.7282 - 0.1083x_1)] \quad (37)$$

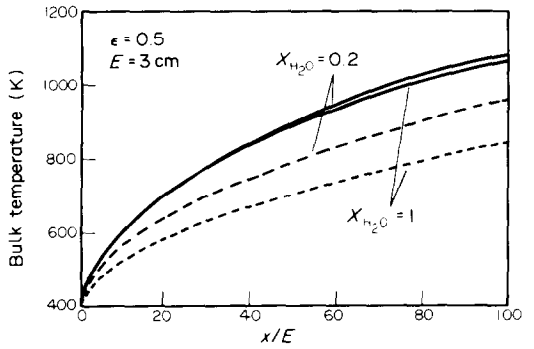

FIG. 3. Bulk temperature evolution for H_2O–air mixture; dotted curves correspond to calculations without radiation.

$$Z = F + GT^m. \tag{38}$$

The state equation for a perfect gas is used to calculate density.

4. RESULTS

The following calculations are performed for H_2O–air mixtures flowing between two parallel walls of constant emissivity. When the fluid is heated, reference temperatures are $T_0 = 400\,K$ and $T_w = 1200\,K$. When the fluid is cooled, $T_0 = 1200\,K$ and $T_w = 400\,K$. Optical thickness of the medium is modulated by adjusting the water vapour molar fraction x_{H_2O} and the distance E between the walls. The mass flow rate per unit area $\dot{m}$ is calculated in such a manner that the Reynolds number, based on the mean temperature of 800 K, remains equal to 2500.

4.1. *Temperature, velocity and radiative flux fields*

Figure 3 shows the evolution of the bulk temperature

$$T_b = \frac{\int_0^E \rho C_p u T \mathrm{d}y}{\int_0^E \rho C_p u \,\mathrm{d}y} \tag{39}$$

along the x abscissa, in the case of a heated mixture with $E = 3\,cm$, $\dot{m} = 1.3\,kg\,m^{-2}\,s^{-1}$, $x_{H_2O} = 0.2$ and 1, and for an established velocity profile at the inlet. Curves with dotted lines correspond to calculations without radiation. It appears that radiation always reduces the difference $(T_w - T_b)$. The molar fraction x_{H_2O} seems to have little effect on the bulk temperature calculated with radiation. This is due to the very different thermophysical properties of the two mixtures; more precisely, the specific heat of water vapour is nearly two times greater than that of air. In order to remove this ambiguity, only pure water vapour flow results will be presented below.

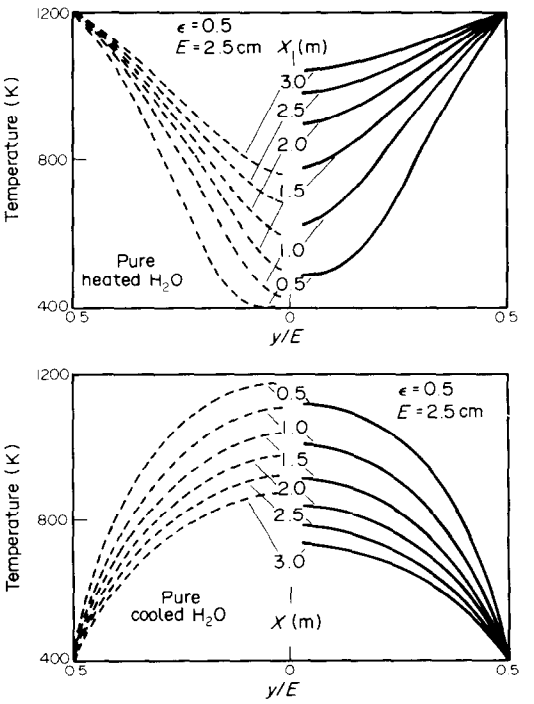

FIG. 4. Temperature profiles: ——,with radiation; – – –, and without radiation; at different downstream locations (x).

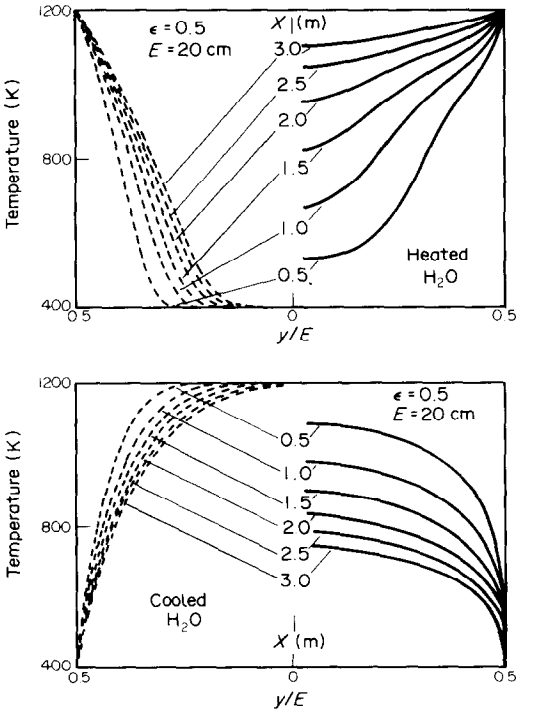

FIG. 5. Temperature profiles: ——, with radiation; and – – –, without radiation; at different downstream locations (x).

Temperature profiles along the axial direction are shown in Figs. 4 and 5. Four cases, corresponding to calculations with and without radiation, for heating

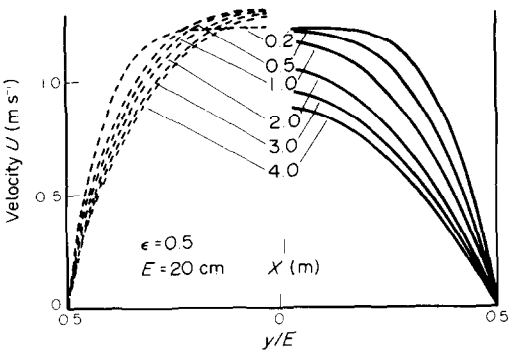

FIG. 6. Dynamic establishment of the flow: ——, with radiation; and – – – –, without radiation; cooled H_2O case.

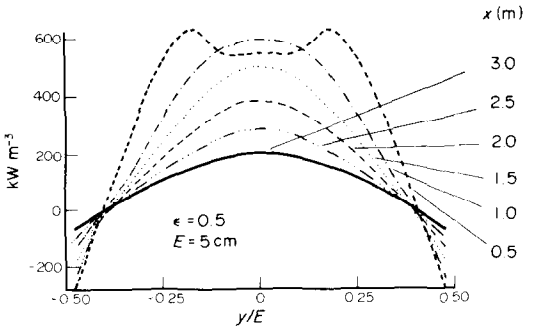

FIG. 7. Transverse radiative dissipation in the case of heated fluid.

and for cooling the fluid, are presented in each of these figures. The velocity inlet profile is parabolic, equation (7), and the channel thickness is 2.5 and 20 cm in the cases of Figs. 4 and 5, respectively. Pure H_2O absorption spectra for these two column lengths and for the limiting temperatures 400 and 1200 K, are presented in Fig. 1. Temperature profile shapes are not appreciably modified by radiation when the medium is not very thick (Fig. 4); the temperature gradient at the wall is diminished in this case for both heated and cooled fluids. This classical result [13, 25] is explained by the fact that the difference $(T_w - T_b)$ is lower in the presence of radiation while the dimensionless temperature $(T_w - T)/(T_w - T_b)$ is not appreciably affected. In the case of Fig. 5, optical paths become important and gas–gas radiation tends to make the temperature uniform at the centre region of the flow; that leads to very important gradients at the wall. Near the entrance region, this wall temperature gradient is greater than that obtained with pure convection, but the result is reversed far away from the inlet because of the very small value of the difference $(T_w - T_b)$.

The temperature profiles obtained for a thick medium are different in the two cases of heated and cooled fluid. In the first case, the region just near the wall is strongly heated by direct absorption of wall radiation which leads to the appearance of two inflection points on the temperature profile; in the cooled gas case, there are no inflection points since the gas itself is the heat source. Finally it is worthy of notice that radiation accelerates thermal development in all cases.

Radiation has no influence on the establishment and on the shape of velocity profiles. This is shown for example in Fig. 6 for the cooled gas case and for a uniform velocity profile at the inlet cross-section. In fact, as pointed out by Im and Ahluwalia [25], radiation effects on the velocity field are only due to variations of ρ and μ with temperature, since radiation pressure is negligible.

Profiles obtained for the radiative dissipation term $\partial q_{Ry}/\partial y$ corresponding to different values of E have similar shapes. The absolute values of $\partial q_{Ry}/\partial y$ first decrease rapidly with E, and then slowly. Figure 7 shows the evolution of this radiative dissipation term for heated water vapour with $E = 5$ cm. Near the channel entrance, the maximum of $\partial q_{Ry}/\partial y$ is located between the flow centre and the wall in this case; in fact, the temperature profile at the centre flow region is still uniform and a relatively cold gas layer exists just near the layer directly heated by the wall. This phenomenon does not appear when the fluid is cooled. It is worth noticing on Fig. 7 the existence of a radiative boundary layer near the wall where hot gas emits more radiation than it absorbs. The thickness of this layer does not vary appreciably along the flow. A similar radiative boundary layer is found when the fluid is cooled; the cold gas near the wall absorbs more radiation, coming from the flow centre region, than it emits.

4.2. *Heat transfer*

Conductive, total and radiative fluxes (φ_{cd}, φ_t and φ_R, respectively) transfered by wall unit area between the wall and the fluid are given by

$$\varphi_{cd} = -\lambda(T_w)\left(\frac{\partial T}{\partial y}\right)_{y=0} \tag{40}$$

$$\varphi_t = \tfrac{1}{2}\int_0^E \rho C_p u \frac{\partial T}{\partial x} dy \tag{41}$$

$$\varphi_R = \varphi_t - \varphi_{cd}. \tag{42}$$

The coefficient $\frac{1}{2}$ in equation (41) accounts for the transfer with the two walls. Flux results are frequently given in terms of conductive, radiative, and total Nusselt numbers; but depending on the temperature used for the evaluation of these Nusselt numbers, the conclusions may be quite different. Results will then be presented here in terms of heat transfer coefficients, i.e. $\varphi/(T_w - T_b)$. Figure 8 shows the evolution of radiative, conductive and total heat transfer coefficients and of the convective coefficient obtained in the absence of radiation, for $E = 5$ cm. The two cases of heated and cooled pure water vapour are illustrated in this figure. Figure 9 shows the same evolution for the optically thicker medium corresponding to $E = 20$ cm. In any case, radiation effects

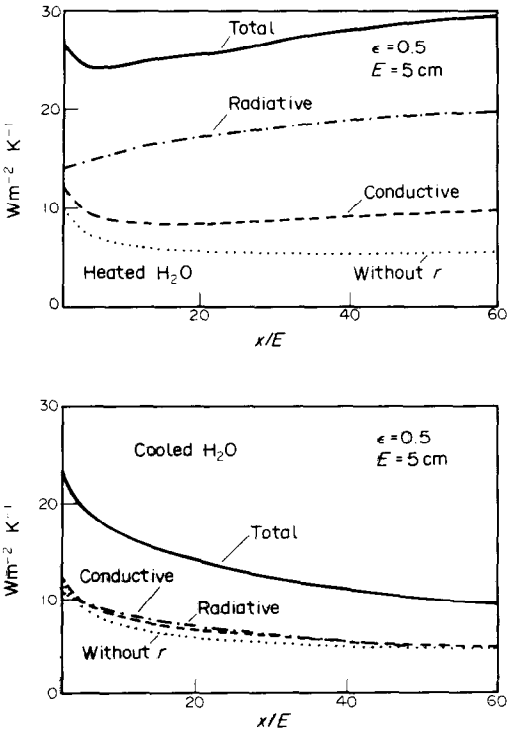

FIG. 8. Total, radiative, conductive and without radiation, heat transfer coefficients.

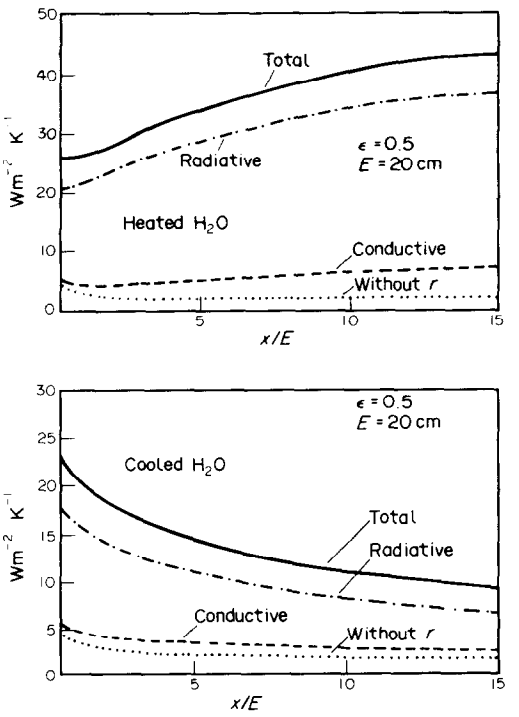

FIG. 9. Total, radiative, conductive and without radiation, heat transfer coefficients.

increase the conductive transfer coefficient, even if the conductive flux is sometimes diminished. As mentioned before, this is due to radiation that tends

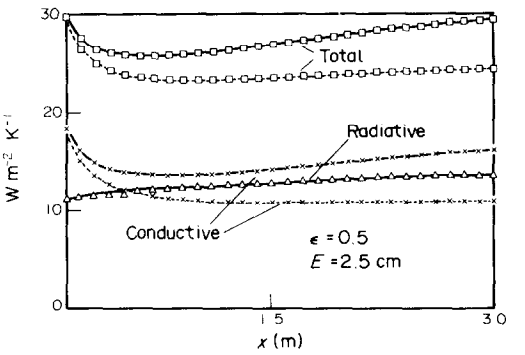

FIG. 10. Total, radiative and conductive heat transfer rates; dotted curves are obtained with thermophysical properties evaluated at 800 K.

to make the temperature profile uniform at the centre flow region, and so, increases the temperature gradient at the wall. The two cases of heated and cooled fluid lead to different results; in the first case, the conductive heat transfer coefficient goes through a minimum at a certain downstream location (as pointed out by Azad and Modest [26]), while the radiative transfer rate increases monotonically. In the case of hot fluid and cold walls, all heat transfer coefficients decrease monotonically and tend to asymptotic values. In a general way, for the same values of $|T_w - T_0|$ and $(T_w + T_0)/2$, radiative heat transfer is greater when the fluid is heated than when cooled. In fact, the absorption coefficient decreases with temperature near the band centres, in spite of the hot absorption bands which lead to an increase of band widths at high temperature (see Fig. 1).

The influence of temperature-dependent thermophysical properties on heat transfer coefficients is shown in Fig. 10 for heated water vapour with $E = 2.5$ cm. Previous results are compared to those obtained when all the physical properties, except radiative ones, are calculated at the mean temperature, 800 K. The radiative transfer coefficient is not appreciably affected, but, as the bulk temperature is lower with constant thermophysical properties, the radiative flux is overestimated. When the strong variations of H_2O thermal conductivity with temperature are not taken into account, wall conductive flux errors up to 35% are obtained.

4.3. *Comparison of wide-band results with statistical narrow-band results*

Calculations based on the statistical narrow-band model consumes more computer time than those using wide-band models, which assume radiative properties to be constant over a whole absorption band. The aim of this section is to show some limits of the use of wide-band models in heat transfer calculations.

Comparisons are made for real H_2O flows with a large temperature difference between the walls and the gas. The wide-band model chosen is the classical

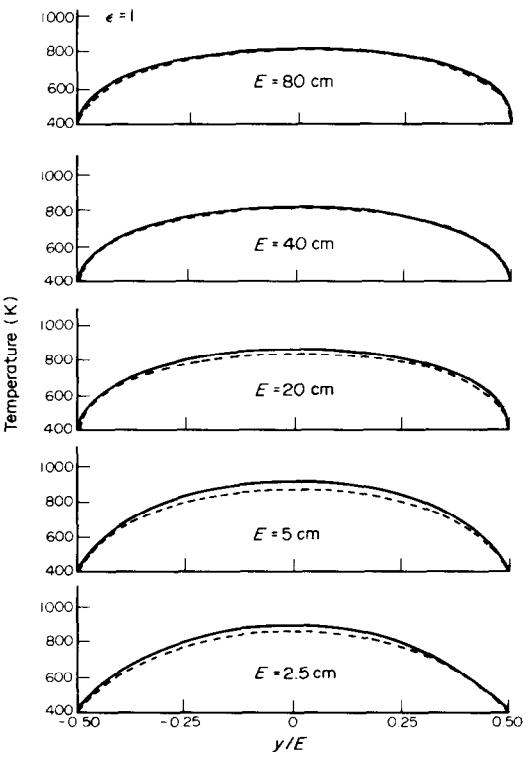

FIG. 11. Temperature profiles at downstream location $x = 1.5$ m: ——, narrow-band results; – – – –, exponential wide-band results.

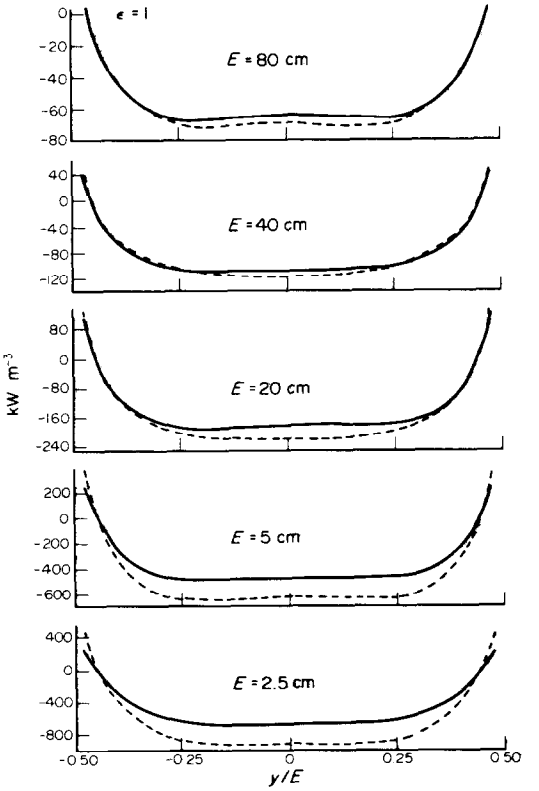

FIG. 12. Radiative dissipation at downstream location $x = 0.2$ m: ——, narrow-band results; – – – –, exponential wide-band results.

exponential-tailed model due to Edwards and the method explained in ref. [33] is strictly used; in particular, equations (196)–(198) are used to approximate radiation from non-isothermal gases. The H_2O absorption bands, considered for both the narrow- and wide-band calculations are those centred at 1.8, 2.7, 6.3 μm and the rotational band. For the latter, the wave-number location ν_k is set equal to 500 cm^{-1} as suggested in ref. [12]. Comparisons are carried out for black walls in order to remove the difficulty which is inherent to the use of the exponential wide-band model for non-black wall calculations.

Figures 11 and 12 show, the temperature and the radiative dissipation profiles respectively, at fixed downstream locations, while Fig. 13 is related to the evolution of the radiative transfer coefficient $(\varphi_R/|T_b - T_w|)$ vs x. These three figures are related to the cooled H_2O case with a channel thickness E growing from 2.5 to 80 cm.

A difference up to 50 K between the wide- and the narrow-band temperature profiles is observed in Fig. 11 for intermediate channel thicknesses. On the other hand, it is obvious that in the two limits of optically thin medium (predominance of convective transfer) and optically thick medium (weak penetration depth of radiation), the two models lead to similar results.

For the radiative flux divergence $\partial q_{Ry}/\partial y$, discrepancies up to 35% between narrow- and wide-band results can be observed in the conditions of Fig.

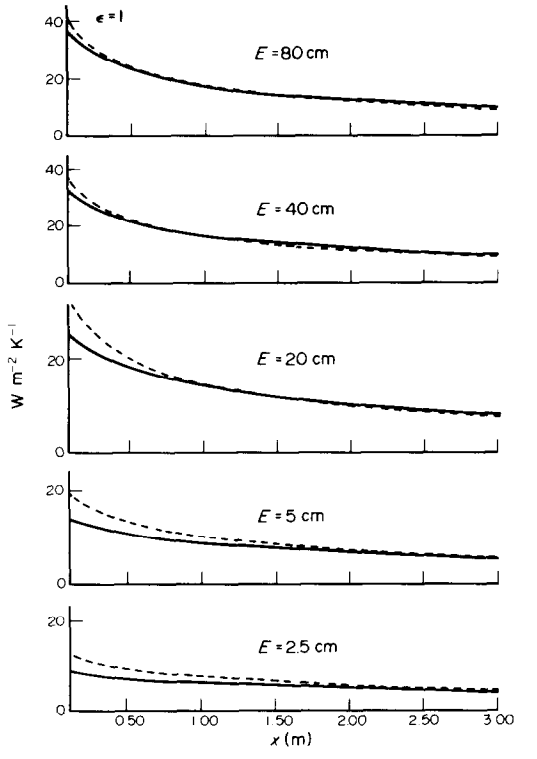

FIG. 13. Evolution of the radiative transfer coefficient: ——, narrow-band model; – – – –, exponential wide-band model.

12. The exponential wide-band model overestimates absorption and emission from water vapour. A similar conclusion is drawn from Fig. 13; substantial deviations are found for the radiative transfer coefficient, in particular, near the entrance of the channel ($x \leqslant 0.5$ m) while temperature profiles obtained with the two models are practically identical. Conductive fluxes at the walls are not appreciably modified when the wide-band model is used.

Results similar to those presented in Figs. 11–13 are obtained when water vapour is heated. Comparisons given in this section are representative of the accuracy of wide-band models for the temperature range used in this study.

5. CONCLUDING REMARKS

A statistical narrow-band model has been applied to the coupled conductive, radiative and convective problem in a laminar flow of emitting and absorbing H_2O–air mixtures, between two parallel and isothermal walls. The conclusions of this study are given below.

(1) Radiation affects the dynamic flow field only through density and viscosity variations with temperature. The shape of the velocity profile remains unchanged.

(2) An important temperature profile modification is observed when the medium is optically thick in the absorption bands.

(3) Radiation generally increases the conductive transfer coefficient as it tends to homogenize temperature in the flow centre region.

(4) Appreciably different results, both for temperature profiles and for heat transfer rates, are obtained when heating and when cooling the fluid. When the values of inlet temperature and wall temperature are permuted, the cold gas and hot wall case leads to the greatest radiative transfer because the mean absorption coefficient is greater at low temperature.

(5) In the two cases, a radiative boundary layer exists near the wall; inside this layer, the strong temperature gradient makes the sign of the radiative dissipation term opposite to that obtained at the centre flow region.

(6) The exponential wide-band model results have been compared to those of the statistical narrow-band model in a large range of optical thicknesses. The most important discrepancies are observed when the optical thickness of the medium is intermediate.

Acknowledgements—The calculations presented in this paper were performed on an IBM 4341 made available to us by the IBM Co.

REFERENCES

1. R. Viskanta, Interaction of heat transfer by conduction, convection and radiation in radiating fluid, *J. Heat Transfer* **85**, 318–328 (1963).
2. Y. Kurosaki, Heat transfer by simultaneous radiation and convection in an absorbing and emitting medium in a flow between parallel plates, *Fourth International Heat Transfer Conference*, Vol. III, paper R2.5, Paris–Versailles (1970).
3. Y. Kurosaki, Radiation heat transfer in a flow between parallel flat plates with temperature slips at walls, *Fifth International Heat Transfer Conference*, Vol. I, pp. 98–102, Tokyo (1974).
4. T. J. Chung and J. Y. Kim, Two-dimensional, combined-mode heat transfer by conduction, convection, and radiation in emitting, absorbing and scattering media–solution by finite elements, *J. Heat Transfer* **106**, 448–452 (1984).
5. R. Greif and D. M. McEligot, Influence of optically thin radiation on heat transfer in the thermal entrance region of a narrow duct, *J. Heat Transfer* **93**, 473–475 (1971).
6. P. S. Larsen and H. A. Lord, Convective and radiative heat transfer to water vapor in uniformly heated tubes, *Fourth International Heat Transfer Conference*, Vol. III, paper R2.6, Paris–Versailles (1970).
7. C. S. Landram, R. Greif and I. S. Habib, Heat transfer in turbulent pipe flow with optically thin radiation, *J. Heat Transfer* **91**, 330–336 (1969).
8. D. K. Edwards and A. Balakrishnan, Nongray radiative transfer in a turbulent gas layer, *Int. J. Heat Mass Transfer* **16**, 1003–1015 (1973).
9. S. De Soto, Coupled radiation, conduction, and convection in entrance region flow, *Int. J. Heat Mass Transfer* **11**, 39–54 (1968).
10. A Balakrishnan and D. K. Edwards, Established laminar and turbulent channel flow of radiating molecular gas, *Fifth International Heat Transfer Conference*, Vol. 1, pp. 93–97, Tokyo (1974).
11. A. T. Wassel and D. K. Edwards, Molecular gas radiation in a laminar or turbulent pipe flow, *J. Heat Transfer* **98**, 101–107 (1976).
12. A. Balakrishnan and D. K. Edwards, Molecular gas radiation in the thermal entrance region of a duct, *J. Heat Transfer* **101**, 489–495 (1979).
13. D. M. Kim and R. Viskanta, Interaction of convection and radiation heat transfer in high pressure and temperature steam, *Int. J. Heat Mass Transfer* **27**, 939–941 (1984).
14. I. S. Habib and R. Greif, Heat transfer to a flowing non-gray radiating gas: an experimental and theoretical study, *Int. J. Heat Mass Transfer* **13**, 1571–1582 (1970).
15. Z. Chiba and R. Greif, Heat transfer to steam flowing turbulently in a pipe, *Int. J. Heat Mass Transfer* **16**, 1645–1648 (1973).
16. D. R. Jeng, E. J. Lee and K. J. De Witt, A study of two limiting cases in convective and radiative heat transfer with non gray gases, *Int. J. Heat Mass Transfer* **19**, 589–596 (1976).
17. R. Greif, Laminar convection with radiation: experimental and theoretical results, *Int. J. Heat Mass Transfer* **21**, 477–480 (1978).
18. D. K. Edwards and W. A. Menard, Comparison of models for correlation of total band absorption, *Appl. Optics* **3**, 621–625 (1964).
19. C. L. Tien and J. E. Lowder, A correlation for total band absorptance of radiating gases, *Int. J. Heat Mass Transfer* **9**, 698–701 (1966).
20. C. L. Tien, Thermal radiation properties of gases, *Advances in Heat Transfer*, Vol. 5, pp. 254–324. Academic Press, New York (1968).
21. L. D. Nichols, Temperature profile in the entrance region of an annular passage considering the effects of turbulent

convection and radiation, *Int. J. Heat Mass Transfer* **8**, 589–607 (1965).
22. J. Taine, A line by line calculation of low-resolution radiative properties of CO_2–CO-transparent nonisothermal gas mixtures up to 3000 K, *J. Quant. Spectrosc. Radiat. Transfer* **30**, 371–379 (1983).
23. J. M. Hartmann, R. Levi Di Leon and J. Taine, Line by line and narrow band statistical model calculations for H_2O, *J. Quant. Spectrosc. Radiat. Transfer* **32**, 119–127 (1984).
24. A. Soufiani, J. M. Hartmann and J. Taine, Validity of band-model calculations for CO_2 and H_2O applied to radiative properties and conductive–radiative transfer, *J. Quant. Spectrosc. Radiat. Transfer* **33**, 243–257 (1985).
25. K. H. Im and R. K. Ahluwalia, Combined convection and radiation in rectangular ducts, *Int. J. Heat Mass Transfer* **27**, 221–231 (1984).
26. F. H. Azad and M. F. Modest, Combined radiation and convection in absorbing, emitting and anisotropically scattering gas–particulate tube flow, *Int. J. Heat Mass Transfer* **24**, 1681–1698 (1981).
27. M. M. Razzaque, D. E. Klein and J. R. Howell, Finite element solution of radiative heat transfer in a two-dimensional rectangular enclosure with gray participating media, *J. Heat Transfer* **105**, 933–936 (1983).
28. S. V. Patankar and D. B. Spalding, A calculation procedure for heat, mass and momentum transfer in three dimensional parabolic flows, *Int. J. Heat Mass Transfer* **15**, 1787–1806 (1972).
29. M. Abramowitz and I. A. Stegun, *Handbook of Mathematical Functions*. Dover, New York (1965).
30. R. C. Reid and T. K. Sherwood, *The Properties of Gases and Liquids*, Chemical Engineering Series, 2nd edn. McGraw-Hill, New York (1966).
31. Y. S. Touloukian, P. E. Liley and S. C. Saxena, *Thermophysical Properties of Matter*, Vol. 3. IFI/Plenum, New York–Washington (1970); and Y. S. Touloukian, S. C. Saxena and P. Hestermans, *Thermophysical Properties of Matter*, Vol. 11. IFI/Plenum, New York–Washington, Copyright (1975).
32. K. W. Shade and D. M. McEligot, Cartesian Graetz problem with air property variation, *Int. J. Heat Mass Transfer* **14**, 653–666 (1971).
33. D. K. Edwards, Molecular gas band radiation, *Advances in Heat Transfer*, Vol. 12, pp. 115–193. Academic Press, New York (1976).

APPLICATION DES MODELES STATISTIQUES A BANDES ETROITES AU COUPLAGE CONVECTION RAYONNEMENT A TEMPERATURE ELEVEE

Résumé—L'utilisation des modèles à bandes larges ou de gaz gris dans des calculs de transferts couplés conduit fréquemment à des erreurs importantes dues aux corrélations spectrales entre émission, transmission et absorption par le gaz. Dans cette étude, un modèle statistique à bandes étroites à loi de distribution inverse-exponentielle des intensités et l'approximation de Curtis–Godson, sont utilisés avec une discrétisation spectrale de 25 cm^{-1}; nos paramètres sont engendrés à partir d'un calcul raie par raie. Les équations dynamiques et l'équation de conservation de l'énergie sont résolues simultanément dans le cas d'un écoulement gazeux entre deux parois parallèles à température imposée. L'influence des variations des propriétés thermophysiques et radiatives avec la température est analysée pour des mélanges H_2O–air, soumis à des gradients importants de température. Un vaste domaine d'épaisseurs optiques est étudié. Des profils de température et de flux thermique différents sont obtenus lorsque les parois sont chauffées ou refroidies. Enfin, les résultats obtenus avec notre modèle statistique à bandes étroites et un modèle exponential à bandes larges sont comparés.

ANWENDUNG EINES STATISTISCHEN SCHMALBANDMODELLS AUF DIE GEKOPPELTEN VORGÄNGE VON STRAHLUNG UND KONVEKTION BEI HOHER TEMPERATUR

Zusammenfassung—Die Verwendung eines Breitband- oder Graugasmodells in gekoppelten Wärmeübertragungsberechnungen führt vielfach zu bedeutenden Fehlern, die auf spektrale Korrelationen zwischen der Intensität der Emission und der Gastransmission zurückzuführen sind. In der vorliegenden Untersuchung werden das statistische Zufallsschmalbandmodell mit dem inversen exponentiellen Flankenabfall und die Curtis–Godson-Näherung benutzt, bei einer Spektralauflösung von 25 cm^{-1}; die Parameter werden mittels einer Zeile-für-Zeile-Berechnung erzeugt. Die gekoppelten Bewegungs- und Energiegleichungen werden für einen emittierenden und absorbierenden laminaren Gasstrom zwischen zwei parallelen Wänden mit konstanter Temperatur gelöst. Die Temperaturabhängigkeit der Strahlungs- und der thermophysikalischen Eigenschaften wird für H_2O–Luft-Mischungen bei großen Temperaturgradienten analysiert. Ein großer Bereich der optischen Dicke wird untersucht. Verschiedene Profile von Temperatur und Wärmestromdichte treten auf, wenn die Wände geheizt oder gekühlt werden. Schließlich werden die Ergebnisse aus dem statistischen Schmalbandmodell und dem exponentiellen Breitbandmodell verglichen.

ПРИМЕНЕНИЕ СТАТИСТИЧЕСКОЙ УЗКОПОЛОСНОЙ МОДЕЛИ К СОВМЕСТНОМУ РАДИАЦИОННОМУ И КОНВЕКТИВНОМУ ПЕРЕНОСУ ПРИ ВЫСОКОЙ ТЕМПЕРАТУРЕ

Аннотация—Применение широкополосных моделей или моделей серого газа в расчетах смешанного теплообмена часто приводит к значительным ошибкам из-за спектральных корреляций между интенсивностью радиационного потока и коэффициентом пропускания газа. В работе используются статистическая узкополосная модель с распределением, имеющим экспоненциальный хвост, и приближение Кертиса–Годсона со спектральным разрешением 25 $см^{-1}$; параметры модели получены на основе расчета для линий. Уравнения движения и энергии решаются совместно для излучающего и поглощающего ламинарного газового потока между двумя параллельными стенками при заданной температуре. Влияние вызванных температурой изменений радиационных и теплофизических свойств анализируется для смеси H_2O–воздух при больших температурных градиентах. Исследуется большой диапазон оптических толщин. Найдены профили температуры и теплового потока при нагреве и охлаждении стенок. Сравниваются результаты, полученные с помощью статистической узкополосной и экспоненциальной широкополосной моделей.